

Measurement infrastructure for the metrological characterisation of single photon sources at European National metrology institutes

S. Kück^{1,2,*}, M López¹, H. Georgieva¹, J. Christinck^{1,2}, G. Porrovecchio³, M. Šmid³, S. Göttinger^{4,5}, C. Becher⁶, P. Fuchs⁶, Pietro Lombardi⁷, Costanza Toninelli⁷, I. P. Degiovanni⁸, P. Traina⁸, S. Rodt⁹, S. Reitzenstein⁹, T. Kübarsepp¹⁰, M. Korpusenko¹⁰, P. Dolan¹¹, C. Chunnillal¹¹, F. Manoocheri¹²

¹ Physikalisch-Technische Bundesanstalt (PTB), Braunschweig, Germany

² Laboratory for Emerging Nanometrology, Braunschweig, Germany

³ Český Metrologický Institut (CMI), Okružní 31, 63800 Brno, Czech Republic

⁴ Department of Physics & Graduate School in Advanced Optical Technologies (SAOT), Friedrich Alexander University (FAU) Erlangen-Nürnberg, 91052 Erlangen, Germany

⁵ Max Planck Institute for the Science of Light, 91058 Erlangen, Germany

⁶ Universität des Saarlandes, Fachrichtung Physik, Campus E2.6, 66123 Saarbrücken, Germany

⁷ Istituto Nazionale di Ottica (CNR-INO), Florence, Italy

⁸ Istituto Nazionale di Ricerca Metrologica (INRiM), Torino, Italy

⁹ Institut für Festkörperphysik, Technische Universität Berlin, Hardenbergstraße 36, 10623 Berlin, Germany

¹⁰ AS Metrosert (Metrosert), Teaduspargi 8, 12618 Tallinn, Estonia

¹¹ National Physical Laboratory (NPL), Hampton Road, Teddington, TW11 0LW, United Kingdom

¹² VTT Technical Research Centre of Finland Ltd, Centre for Metrology MIKES (MIKES), Tekniikantie 1, 02150 Espoo, Finland

* Corresponding author: stefan.kueck@ptb.de

1. Introduction

In this paper we report on the development of measurement infrastructure at European national metrology institutes (NMIs) for the characterization of single-photon sources. The measurement infrastructure reported on is the one developed or further developed, respectively, within the frame of the Joint Research Project SIQUST (Single-photon sources as new quantum standards, 17FUN06 [1]). The setups and devices included detectors, detector characterization setups, transportable single-photon sources, setups for the characterization of the total spectral radiant flux and the photon statistics of single-photon sources as well as laser sources for the operation of single-photon sources.

2. Measurement setups

In the following, the setups developed or further developed within the SIQUST project are listed and described.

2.1. Low optical flux detectors (LOFP)

A Si S1227 33 Hamamatsu Si photodiode is placed in a custom-made aluminium housing. One side of the housing is threaded to accept different type of commercially available fibre connectors. The mechanical set up is designed to place the fibre optic tip at a fraction of millimetre from the photodiode sensitive area to guarantee that all the optical radiation is

collected by the photodiode. The photodiode terminals are connected to a SIA developed by CMI [2] equipped with a 1pF Mica integration capacitor. The value of the capacitor has been calibrated using the method described in [3]. Changing the integration time of the SIA the I/V conversion factor can be set to a value that ranges from 1×10^9 to 1×10^{12} .

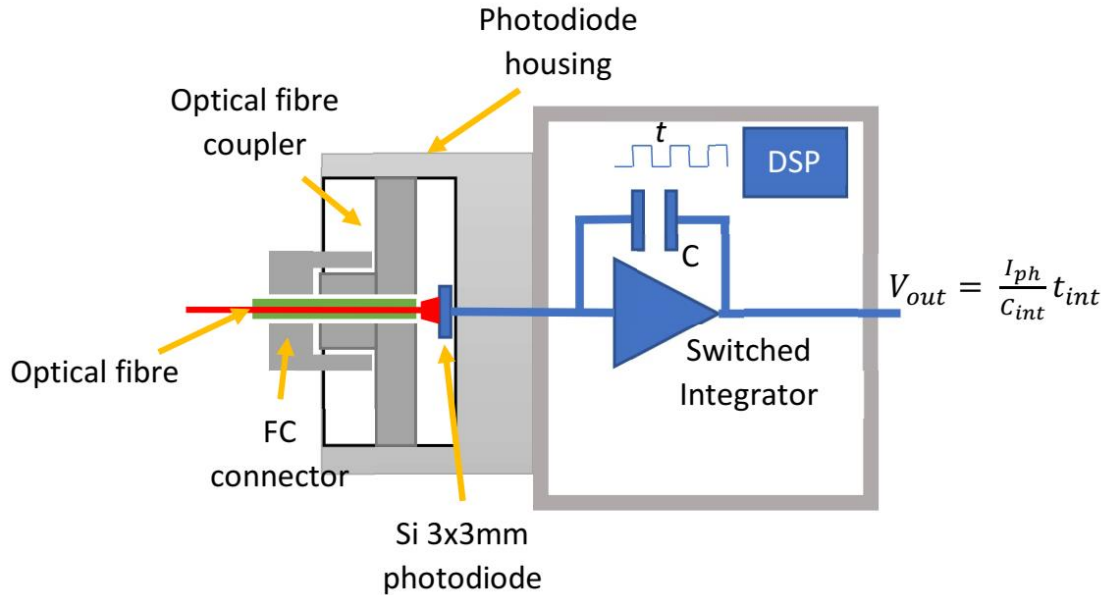


Figure 1. Schema of the low optical flux detector

For a monochromatic source of wavelength λ the number of photons per unit of time impinging the LOFP's photodiode is calculated by the equation

$$N_{Photons/s} = \frac{V_{out} \cdot C_{int}}{R_{\lambda} \cdot t_{int} \cdot e_{\lambda}}$$

Where R_{λ} is the responsivity of the photodiode at λ and e_{λ} is the energy of a photon at λ .

2.1.1 photodiode spectral responsivity

The absolute spectral responsivity of the LOFP's Si photodiode has been calibrated using the CMI double monochromator facility. The LOFP and the CMI Si trap transfer standard detector were alternatively illuminated by the spectrally selected light. The CMI trap detector is directly traceable to the CMI primary standard for optical radiation the cryogenic radiometer. The calibration has been performed in the spectral range 580 – 960 nm with 10 nm step with power levels of few nW in order to not saturate the CMI detector set to its lowest sensitivity. The resulting spectral responsivity is reported in Figure 2. The total extended uncertainty above 900 nm is about 2.2%

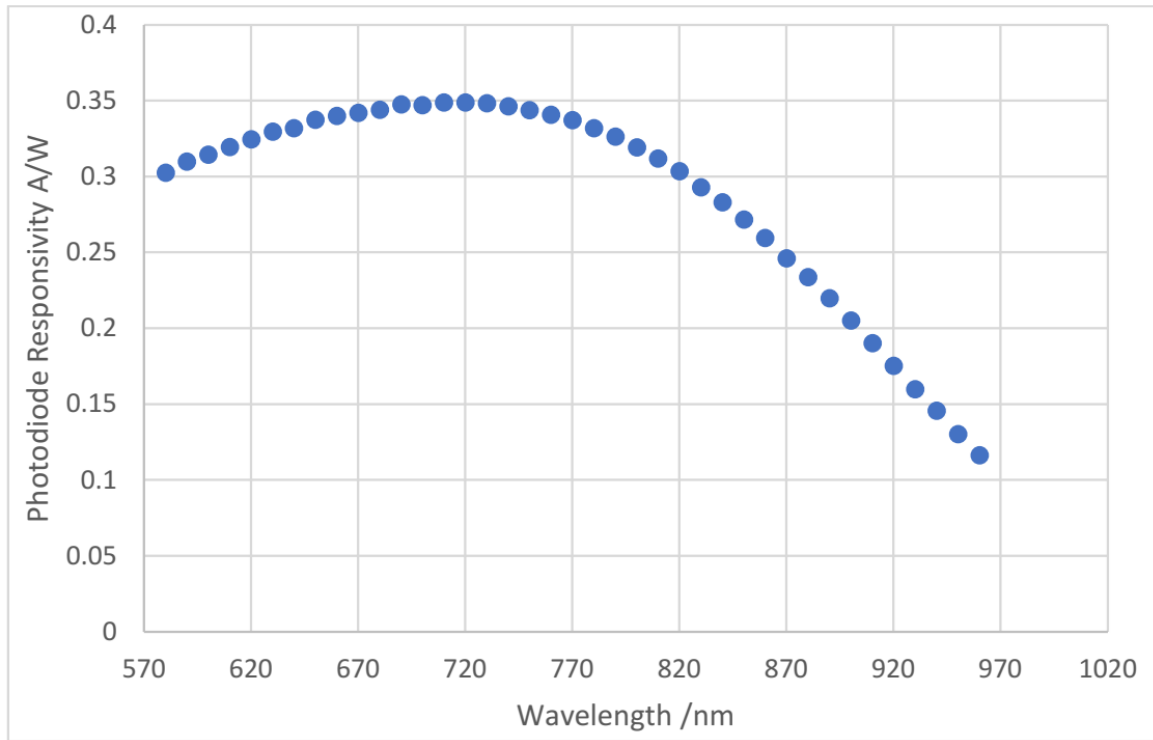


Figure 2. LOFP Si photodiode spectral responsivity

2.1.2 LOFP noise performance measuring SPS

A series of measurements of the photon flux emitted by the PTB SPS were performed with the LOFP at different optical excitation levels for the SPS. In the Table 1 below we report the relative standard deviation of five measurements with the SPS photon flux of about 1.2×10^6 photons/s and 0.4×10^6 photons/s, respectively.

Table 1. Summary of the measurements of the SPS photon flux.

Power /W	# photons/s	Power /W	# photons/s
2.61×10^{-13}	1.22×10^6	9.34×10^{-14}	4.37×10^5
2.57×10^{-13}	1.20×10^6	9.04×10^{-14}	4.23×10^5
2.61×10^{-13}	1.22×10^6	9.17×10^{-14}	4.29×10^5
2.64×10^{-13}	1.23×10^6	9.31×10^{-14}	4.36×10^5
2.60×10^{-13}	1.22×10^6	8.99×10^{-14}	4.21×10^5

Average	1.22×10^6	4.29×10^5
Rel. std. dev.	1.0 %	1.7 %

To notice that the statistical scatter values reported include both the random detector noise and the SPS flux fluctuations. The fact that the total relative noise doesn't scale with the photon flux indicates that the LOFP noise floor contribution is not dominant to the overall measured noise.

2.2. Predictable quantum efficient detector for traceable low optical flux measurements of SPS systems

The predictable quantum efficient detector (PQED) is a primary standard of optical power operating in the visible wavelength range [4, 5, 6]. The PQED consists of two custom-made induced-junction silicon photodiodes [4, 7] arranged in a wedged trap configuration. Over the last decade, the properties of the PQED have been studied comprehensively [4, 5, 6, 8], and the PQED has been applied in various fields of optical metrology [9, 10, 11]. The characterization measurements have shown many appreciable properties, such as high-charge carrier collection efficiency [5, 12], low reflectance [4], and linear response over seven orders of magnitude [5]. The uncertainty in the predicted responsivity of the PQED is below 100 parts per million (ppm) [4, 12, 13].

Originally, all PQED photodiodes were based on a structure of thermally grown silicon oxide (SiO₂) on p-type silicon [4]. Recently, an alternative structure was demonstrated [12], where atomic layer deposition (ALD) was used to grow aluminium oxide (Al₂O₃) on top of n-type silicon. Two sets of n-type silicon induced-junction photodiodes were manufactured, denoted as set A and B, with respective doping concentrations of $2.5 \times 10^{11} \text{ cm}^{-3}$ and $4.4 \times 10^{11} \text{ cm}^{-3}$. In addition to smaller doping concentration, set A photodiodes have 16 guard rings, whereas those of set B have only one. These factors lead to a decrease of dark current by a factor of five at room temperature for the set A photodiodes when compared against set B [12].

Improved dark current characteristics play a major role in low optical flux measurements, as reduced dark current will increase the signal-to-noise ratio (SNR). Additionally, simulations have been carried out to determine dark current behaviour when cooling the photodiodes down to cryogenic temperatures [14, 15]. These simulations indicate that the dark current will decrease exponentially with lowering temperature. Thus, cooling the PQED would drastically increase the dynamic range of the PQED, and would enable the PQED to be used as a primary standard in single and few photon applications [16]. Manoocheri et al., have reported the design of a cryogenic PQED consisting of a liquid nitrogen (LN) cooled cryostat fitted with n-type photodiodes [17]. Porrasmaa et al., have reported the dark current dependence on bias voltage at room temperature for both the n- and p-type PQED photodiodes. The dark current properties of the n-type detector in the temperature range of 76–300 K have also been presented and demonstrated the possibility of using the PQED as a primary standard in low flux applications [18].

2.2.1. Cryostat design

The cryostat and the pumping system used in this study are similar to those described and characterized in [17, 18]. Therefore, only a short description is given here. The schematic drawing of the cryostat design is shown in Figure 3. The cryostat is pumped with a turbomolecular pump together with a mechanical backing pump. A radiation shield enclosing the photodiodes is connected directly to a liquid nitrogen (LN) vessel and serves as a cold trap.

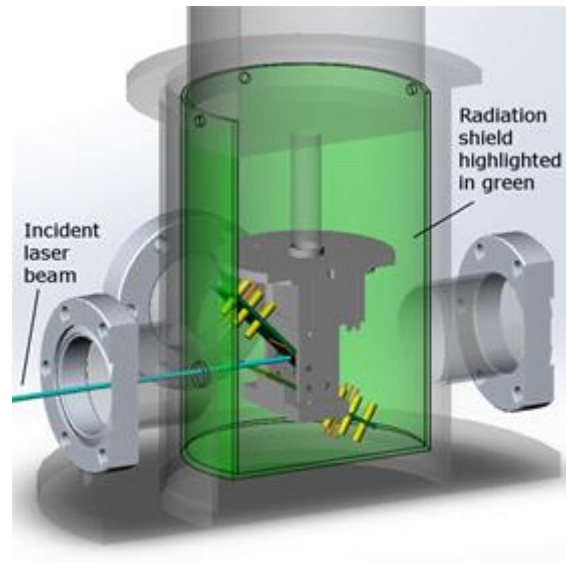


Figure 3. Schematic drawing of the cryostat. The radiation shield has an aperture of 10 mm in diameter for the incident laser beam to reach the photodiodes. The central grey part in the figure serves as the photodiode holder. The dimmed grey part above the holder represents a thermal connection between the photodiode holder and the LN vessel.

The photodiode holder is in a good copper-to-copper thermal connection with the LN vessel to ensure sufficient heat exchange between them, even under vacuum conditions. The photodiode holder can also be electrically heated. The cryostat is also equipped with a heatable charcoal getter to trap permeated gases. In standard operation, a window aligned in Brewster's angle is placed in front of the photodiodes.

When mounted to the photodiode holder, the PQED photodiodes form a wedged trap configuration (see Figure 4), similarly to previously characterized PQEDs [4, 6, 12]. The wedged trap configuration and its properties are thoroughly studied in [19]. Although the reflectance of the n-type detector is higher than that of the p-type, the reduced dark current characteristics of the n-type detector were considered to be more critical in a few photon applications and were thus chosen for this application. The cryostat was fitted with two n-type PQED photodiodes from set A [9]. These photodiodes were glued to carrier chips that were manufactured from a silicon wafer. When cooled, this silicon-on-silicon structure overcomes the problems of previous photodiode designs [4] due to deviating thermal expansion coefficient of the photodiode and the carrier.

To reduce outgassing from the inner surfaces of the cryostat, it was baked—while pumping—at 333 K for 12 h before first cooling. When cooled, a vacuum level of around 20 μPa was achieved.

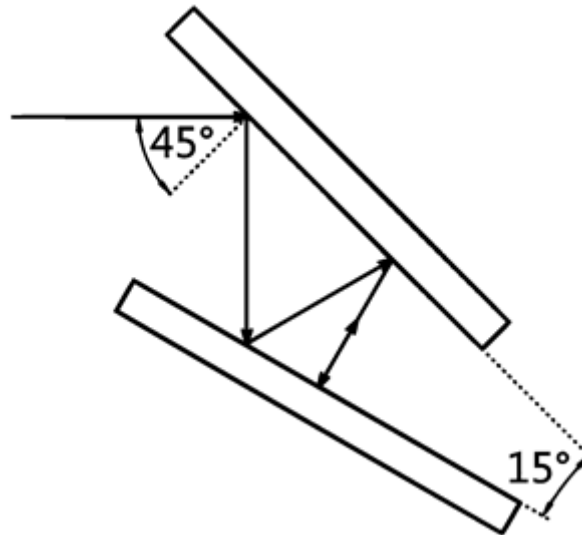


Figure 4. Schematic drawing illustrating the wedged trap configuration of the photodiodes.

The measurements have been carried out with a similar setup as described in [12] with the addition of the cryostat on the XY-translation stage and neutral density (ND) filters for attenuating the incident laser beam as shown in Figure 5. For measuring the dark current and low flux photocurrent, the photodiodes were connected to a precision, gain-controllable, commercial transimpedance amplifier (TIA). Two ND filters with nominal optical densities of 3.0 and 4.0 were used to reduce the power of the stabilized laser beam down to 2.8 pW. This corresponds to roughly 7,000,000 photons per second at a vacuum wavelength of 488.12 nm. While the responsivity simulation of the PQED assumes reverse bias [13], at such a small power level, the uncertainty due to non-biased operation is significantly less than the uncertainty of the measurements [12]. Thus, the photodiodes were not biased. This increased the SNR (lowers the noise floor) significantly. In optical power measurement at 76 K and without biasing, a relative standard uncertainty of 0.15% was achieved within a 5-min measurement period.

2.2.2. Experimental setup

To investigate properties of the cooled PQED, we executed following measurements such as spatial uniformity scanning of the detector responsivity, detector reflectance measurements, responsivity measurements against p-type PQED and measurement of photocurrent dependence with and without bias voltage at low incident power levels. The measurement setup (Figure 5) includes two laser sources: an argon-ion laser at 488.12 nm wavelength with a Gaussian-like beam diameter of 1.3 mm ($1/e^2$) and a single longitudinal mode and a semiconductor laser at 933 nm wavelength with a diameter of 2.6 mm of the vertically polarized beam. Both lasers were simultaneously used only when aligning the 933 nm laser beam for reflectance measurements. An optical power stabilizer provided a stable p-polarized laser beam, and a wedge mirror with monitor detector was used for any laser drift correction.

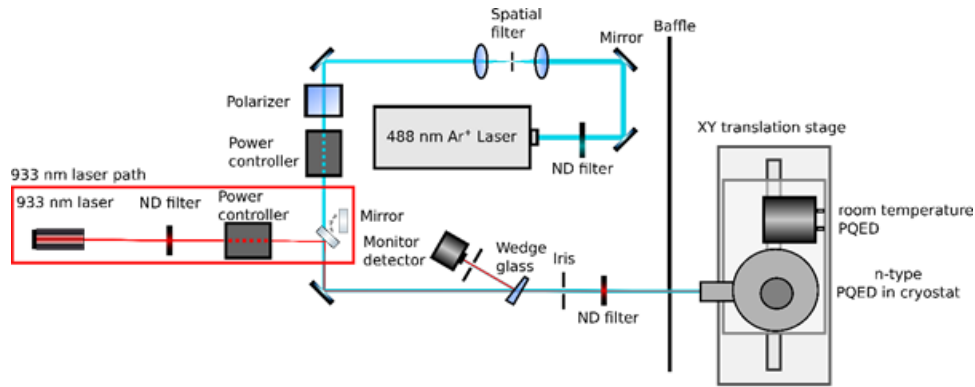


Figure 5. Schematic drawing of setup for optical power responsivity measurement of PQEDs at Aalto.

2.3. Transmission-type photodetectors as alternative attenuator to achieve and monitor of low photon flux

In the establishment of traceability of low photon flux detectors to primary standards (e.g., cryogenic radiometer, Predictable Quantum Efficiency Detector) optical filters or other optical components are often used. One of the drawbacks in using additional optical components is undesired back-reflection, which can cause inter-reflections and stray light in the measurement system and, as a consequence, increase in uncertainty. One way to overcome this is to use special type of attenuators, so-called transmission type detectors.

This part of deliverable D8 describes a testbed which is able to provide collinear input and output beams to better than $\pm 0.5^\circ$ of the transmission type detector that use a slightly cooled ($+12^\circ\text{C}$) transmission type detector and the characterization results at laser wavelengths 647 nm and 676 nm (project activities 4.1.2 and 4.1.3).

2.3.1. Photodiodes

The photodiodes used in the transmission type detector (further called as detector 6X) are Silicon-photodiodes type S1227-33 SPL (windowless) from Hamamatsu with active area $2.4\text{ mm} \times 2.4\text{ mm}$. This type of photodiodes has been proved to operate at low noise and high sensitivity and has been used to establish reliable traceability chain to cryogenic radiometer in low photon flux measurements [3].

2.3.2. Construction

The alignment of six photodiodes was chosen in such a way that it provides almost collinear input and output beams, and transmittance, as well as responsivity are independent on the polarization state of the beam ^[20] (Figure 6a).

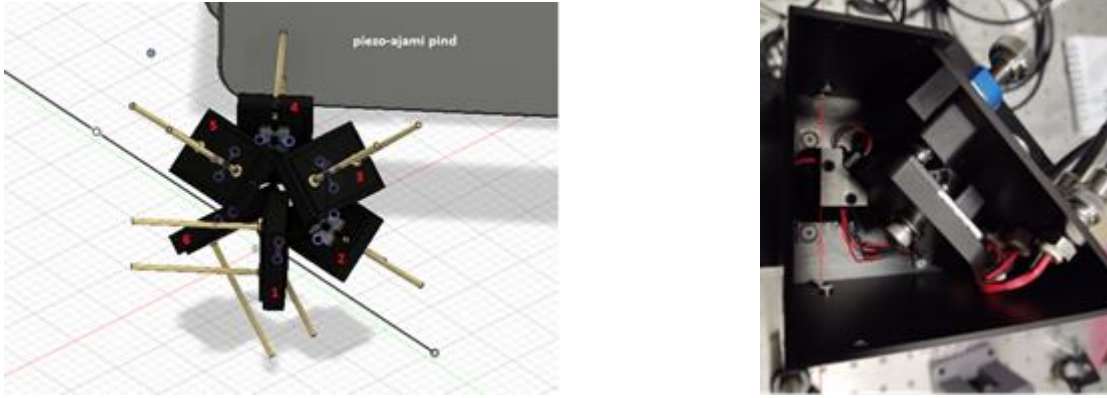


Figure 6a) The schematic isometric view of six photodiodes in the transmission trap detector. b) Top view of the transmission trap detector with the top lid opened.

The configuration of the photodiodes was designed for the shortest optical path 38 mm in the device, limited mostly by photodiode frame dimensions and piezo-mover holding one of the photodiodes for fine tuning purposes of the beam travelling between the photodiode active surfaces (Figure 6b).

The outer housing of the transmission type detector 6X is rectangular shape in which the total optical path is 103 mm.

The Peltier' element type TECL4 in conjunction with thermocontroller TED200C from Thorlabs is used to cool the detector 6X. The feedback thermistor type AD590 is located close to the mechanical body holding the photodiodes in the designed configuration.

2.3.3. Performance

Active area

The active area of the detector 6X was measured by using 676-nm laser wavelength beam with diameter of about 1 mm. The measurements were performed with scan step of 0.25 mm at room temperature. The results are shown in Figure 7. It can be seen that the active area of photodetector 6X is about 1.75 mm (height) and 1.25 mm (width).

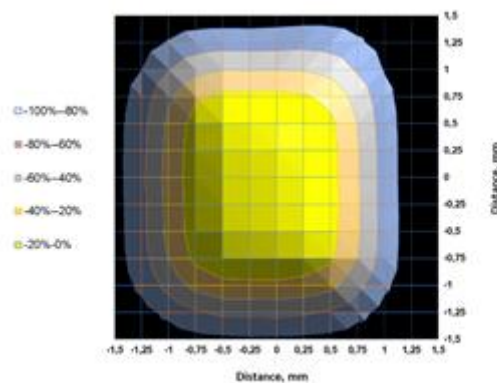


Figure 7. The active area of the photodetector 6X measured with 1-mm diameter laser beam at the wavelength of 676 nm at room temperature.

Transmittance, attenuation

By knowing the thickness of SiO₂ antireflection coating on the top of Si-photodiode active surfaces, the fraction of the incoming beam transmitted through the detector (i.e., attenuated) can be estimated. The previous studies have indicated that the antireflection coating thickness of photodiodes type S1227-33 is $t=(30\pm 1)$ nm [21].

At the laser wavelength of 639 nm

- Expected transmittance is $7.51e-4$, i.e., attenuation is 1331 times,
- Measured transmittance is $7.65e-4$, i.e., attenuation is 1307 times.

The transmittance of the detector 6X was also measured when the device was cooled from room temperature to $+12^{\circ}\text{C}$. The results are presented on Figure 8.

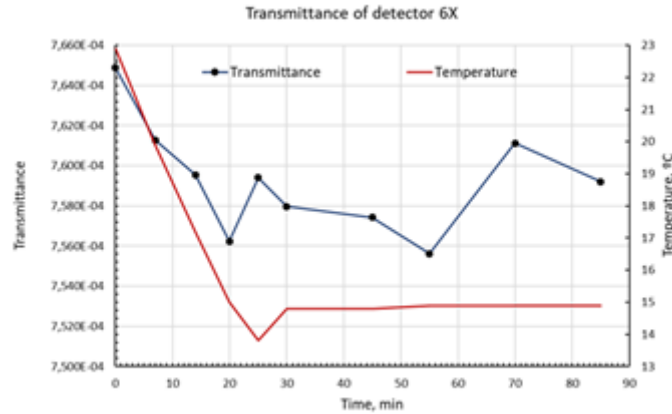


Figure 8. Results of transmittance measurements at the laser wavelength of 639 nm during cooling of the transmission trap detector 6X over 1.5 hours.

It can be seen that the optical power in the transmitted beam drops by about $4e-6$ within first 15 minutes of detector cooling. After that, transmittance is stable to better than $\pm 2e-6$ during 1 hour of cooling process of the detector 6X. This, probably, indicates that the cooling of the detector did not cause significant displacement of the individual photodiodes in the device.

Cooling tests

The photodetector 6X can be cooled from laboratory temperature $+22.9^{\circ}\text{C}$ to $+12^{\circ}\text{C}$ within $1\frac{1}{4}$ hours. The dark current measurements were conducted in the temperature range from $+15^{\circ}\text{C}$ to $+23^{\circ}\text{C}$. The dark current reading from photodiodes 1, 2, 5 and 6 of the photodetector 6X summed up was registered by using conventional current-to-voltage amplifier gain setting 10^9 . The results are depicted in Figure 9. It was measured that the dark current of photodiodes 1, 2, 5 and 6 decreases by about $25\text{ fA}/^{\circ}\text{C}$.

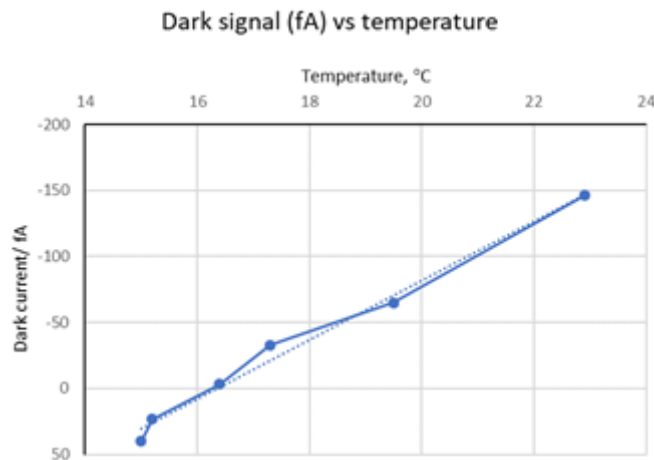


Figure 9. The dark current resulting from photodiodes 1, 2, 5 and 6 summed up as a function of temperature of photodetector 6X.

The total dark photocurrent of the detector 6X was measured at temperatures +15°C and +23°C using different amplifier gain settings: 10^4 , 10^7 and 10^9 . It was observed that dark current of the detector at temperature +15°C is about one order of magnitude less as compared to that at temperature +23°C at three amplifier gain settings.

2.3.4. Characterisation against PQED

The responsivity of the detector 6X was calibrated against PQED at the laser wavelengths of 647 nm and 676 nm by using 1-mm diameter of the laser beam (Figure 10) at Aalto University. The results at different levels of the optical power at two temperatures are listed in Tables 2 and 3.

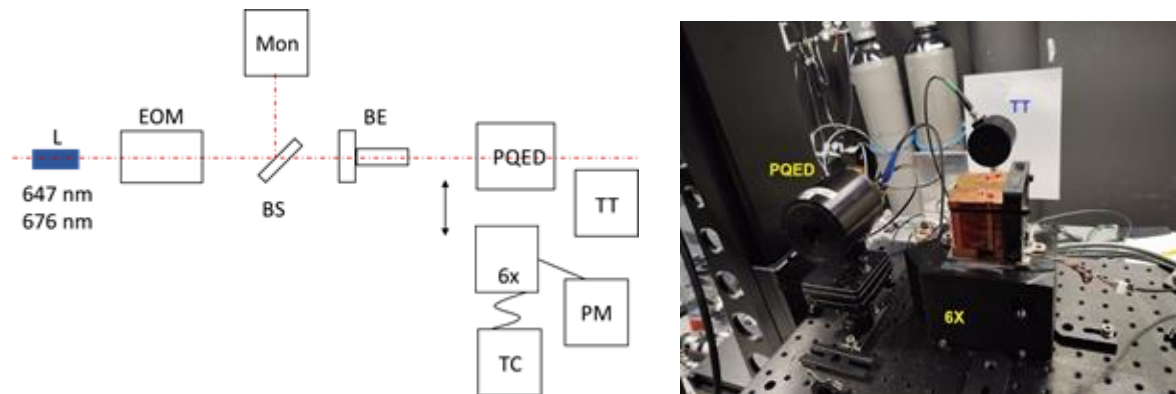


Figure 10. Measurement set-up for the photocurrent ratio measurements of cooled transmission trap detector 6x; TT denotes a conventional 6-element transmission trap detector (available from the EMRP JRP EXL02 SIQUTE); PQED denotes Predictable Quantum Efficiency Detector.

Table 2. Photocurrent ratio i_{6X}/i_{PQED} measurement results at 647-nm laser wavelength.

Optical power	Temperature	Photocurrent ratio with standard uncertainty ($k=1$)
120 uW	RT	0.972 ± 0.004
117 uW	15°C	0.972 ± 0.004
60 uW	RT	0.971 ± 0.004
0.60 uW	RT	0.972 ± 0.004
120 nW	RT	0.970 ± 0.004
60 nW	RT	0.970 ± 0.004
11 nW	15°C	0.968 ± 0.004

Table 3. Photocurrent ratio i_{6X}/i_{PQED} measurement results at 676-nm laser wavelength.

Optical power	Temperature	Photocurrent ratio with standard uncertainty ($k=1$)
120 μ W	RT	0.956 ± 0.004
120 μ W	15°C	0.954 ± 0.004
250 nW	RT	0.955 ± 0.004
245 nW	15°C	0.953 ± 0.004
0.5 nW	15°C	0.957 ± 0.004
0.3 nW	15°C	0.957 ± 0.005

It can be noted that responsivity of detector 6X is stable regardless of the level of optical power and temperature (Tables 2 and 3).

2.3.5. Summary

The ultra-compact transmission trap detector 6X consisting of six photodiodes with active area 2.4 mm x 2.4 mm was designed and manufactured in polarization-independent configuration. The imperfections in photodiode alignment due to mechanical construction can be compensated by moving one photodiode in the device to provide collinear input and output beams. It was observed that the detector is capable of providing and maintaining collinear input and output beams at room temperature and cooled to +12°C. This is a feature which can be exploited in accurate attenuation to provide low photon flux beams. In addition, photocurrent measurements can be conducted separately for 3rd, 4th and 1-2-5-6 photodiodes, which can be useful in monitoring stability of optical power in the laser beam and determination of polarization state of the incoming radiation. When cooled, the dark current of the detector is reduced to sub-picoamp level depending on the gain of the conventional amplifier used.

The transmission-type detector 6X is comparably easy to align into the measurement set-up as the fraction of the incoming beam, which is not absorbed but transmitted, can be observed and its direction tuned, if necessary. However, owing to small active area of the photodiodes, a laser beam diameter less than 1 mm is recommended to use in the measurements.

The detector 6X was calibrated by using Predictable Quantum Efficiency Detector (PQED) [4, 5] at the laser wavelengths 647 nm and 676 nm and at two temperatures. The responsivity of detector 6X was measured to be 0.506 A/W and 0.520 A/W, respectively.

2.4. Single-photon source characterization facilities

2.4.1. Characterization facilities for single-photon sources based on impurity centres in diamond

Diamond as a host medium for single-photon emitters is advantageous because of the mechanical stability and the possibility to generate single-photons at room temperature. Impurity-based centres such as germanium-vacancy, tin-vacancy and nitrogen-vacancy centres

are candidates for applications using single-photon sources at room temperature. These emitters are characterized in a self-built confocal microscope setup, which is illustrated in Figure 11.

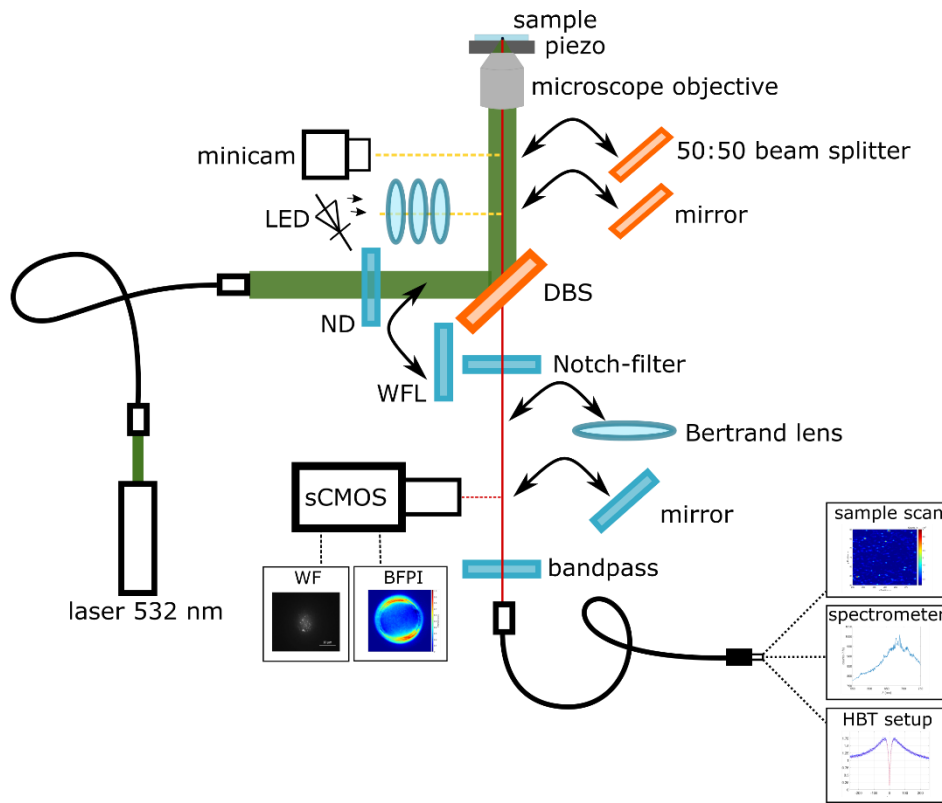


Figure 11. Confocal microscope setup to characterize single-photon emitters in diamond at room temperature. ND: neutral density filter. WFL: wide-field lens. DBS: dichroic beam splitter.

The laser light at 532nm (PicoQuant, LDH-D-FA-530L) with a maximum CW power of up to 5 mW or pulsed operation with up to 80 MHz repetition rate is coupled into the microscope setup using a single-mode optical fibre (Thorlabs, P1-460-FC-2) and attenuated by a neutral density filter wheel called (Thorlabs, NDC-100C-4M). A dichroic beam splitter (Thorlabs, DMLP550) is used to direct the laser onto the microscope objective (Olympus, MPlan Apo N, 50x NA 0.95, can be exchanged with Mitutoyo, M Plan Apo 100x NA 0.7). Using a piezo translation stage (PI, P563.3CD), the sample can be scanned in three dimensions. The fluorescence from the focal volume is gathered by the same microscope objective and filtered by a Notch-filter (Edmund Optics, 532nm Notch-filter, OD6, #86-130) and a bandpass filter (Edmund Optics, 620nm bandpass, 56 nm bandwidth, OD6, #33-910) for germanium-vacancy or tin-vacancy centre samples or long-pass and short-pass filters (Thorlabs, FEL600 and FES700) for nitrogen-vacancy centres. A single-mode optical fibre (Thorlabs, P1-630A-FC-2) is used as the pinhole. The fluorescence is then measured in a single-photon avalanche diode (Laser Components, Count-T-100-FC), a HBT setup consisting of two detectors and a beam splitter (Thorlabs, TW670R5F1) or a spectrometer (Princeton, Spectra Pro SP-2500). The setup also has the possibility for wide-field microscopy of the fluorescence and back focal plane imaging using a sCMOS camera (Andor, Zyla 4.2Plus). An LED and a minicam (Thorlabs, DCU223M) are used to align the sample with the microscope objective.

Nanodiamonds that were spin-coated onto a cover glass emit more than 80% of their photons into the cover glass [22]. The extraction efficiency of the photons from the cover glass is enhanced by using oil-immersion microscope objectives, since no total internal reflection in the cover glass can occur. Therefore, the microscope objective in the setup can be exchanged with an oil-immersion objective (Nikon, CFI Plan Apochromat Lambda 60x Oil).

2.4.2. Characterization facilities for single-photon sources based on InGaAs quantum dots in the near infrared spectral range

Semiconductor quantum dots are robust and mechanically stable. They can endure many cooling cycles, and they do not suffer from blinking and photobleaching. Another advantage is the short decay time on the order of 1 ns which allows for pulsed excitation at high repetition frequencies. In the following, we are applying a nonresonant optical excitation at a frequency of 80 MHz.

A key technique for the optical characterization of semiconductor quantum dots and other quantum emitters in general is confocal fluorescence microscopy. The confocal setup is illustrated by a schematic sketch in Figure 12. The setup transmission is optimized for the emission wavelength of the quantum dots (around 930 nm). Furthermore, the setup is equipped with a helium flow cryostat for cooling the sample to cryogenic temperatures.

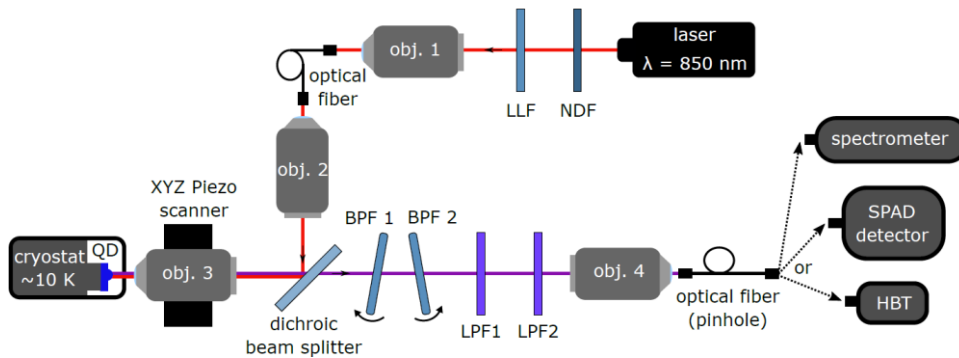


Figure 12. Sketch of the confocal setup for the optical characterization of semiconductor quantum dots emitting at around 930 nm. The excitation beam passes through a neutral density filter (NDF) and a laser line filter (LLF). Then it is reflected at the dichroic beam splitter and focused on the sample by objective 3. The sample is cooled down to about 10 K via a helium flow cryostat. The fluorescent emission is spectrally filtered by two bandpass filters (BPF1 and BPF2) and two long pass filters (LPF1 and LPF2). Objective 4 focuses the light beam into an optical fibre that serves as a pinhole and can be connected to either a spectrometer, a SPAD detector or a Hanbury-Brown and Twiss (HBT) interferometer. Taken from [23].

The excitation laser (PicoQuant, LDH-D-C-850) in pulsed mode has a relatively broad spectral emission, which has to be constrained by a laser line filter (LLF) at 850 ± 10 nm. Moreover, the excitation power is adjusted with a neutral density filter (NDF) wheel (Thorlabs, NDC-100C-4M). The same objective (obj. 3) is used to focus the excitation beam on the sample and to collect the fluorescent emission. A dichroic beam splitter (Semrock, 875 nm edge BrightLine) separates the fluorescent beam from the excitation beam. Two long pass filters (LPF, Thorlabs, FEL0900 and Edmund Optics, high performance OD 4.0) with a cut-off wavelength of 900 nm additionally suppress the laser beam. The spatial filtering in front of the detector is realized by an optical fibre, which has the function of a confocal pinhole that filters out light originating outside the focal spot.

The sample is raster-scanned point by point to construct a two-dimensional fluorescence image, as shown in Figure 13a). The fluorescent light is detected by a single-photon avalanche detector (SPAD) with a sensitivity at the single-photon level. The selected quantum emitter in the scan is placed in focus. Then the optical fibre is connected to a spectrometer to obtain the spectral characteristics. The spectral filtering of the quantum dot emission is realized by two very

narrow bandpass filters (BPF, Alluxa, 935.0–0.45 OD5) mounted on automated rotation stages (PI, RS40 with a Mercury C-863 DC motor controller). We expect a wavelength shift of the central wavelength of the transmission window as a function of the incident angle. This shift is implemented for the spectral selection of a specific emission line with an emission wavelength close to the target value of 930 nm (see Figure 13b).

The last characterization step consists in analysing the single-photon purity by a measurement of the second-order correlation function. This measurement is performed with a Hanbury Brown and Twiss interferometer made of a 50/50 fibre-based beam splitter (Newport, F-CPL-M12855) with multimode fibres having a core diameter of 62.5 μm , two Si-SPADs and electronics (PicoQuant, PicoHarp 300) for time-correlated single-photon counting (TCSPC). The $g^{(2)}(0)$ values at different photon fluxes are shown in Figure 13c. We were able to achieve photon fluxes of up to approx. 2.6 million photons per second at the position of the single-photon detector.

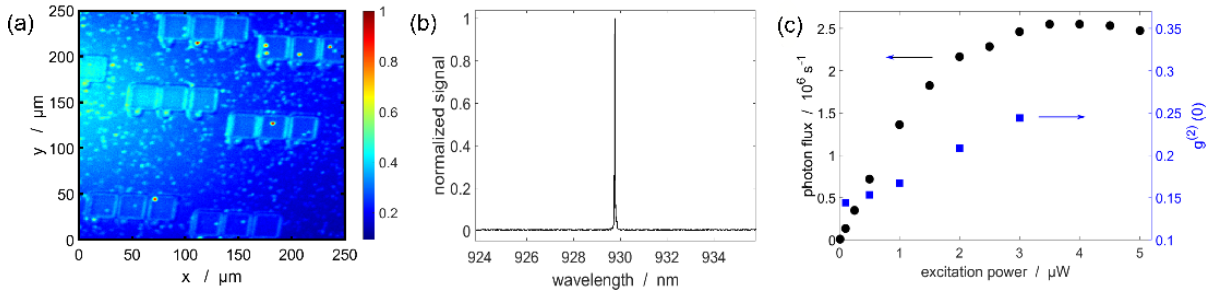


Figure 13. a) Micro-photoluminescence scan of the sample emission. Emission below 900 nm is filtered out by a long pass filter. B) Spectrum of the quantum dot emission with applied spectral filtering. C) The black circles indicate the photon flux arriving at the single-photon detector as a function of the excitation power, whereas the blue circles indicate the corresponding $g^{(2)}(0)$ values. Figure c) is taken from [23].

The metrological characterization requires traceability to the primary standard for optical power, the cryogenic radiometer. Therefore, the use of calibrated SPAD detectors enables absolute measurements of the photon flux and of the corresponding optical power. An important advantage of InAs quantum dots is their narrow-bandwidth emission. A monochromatic emission is an essential prerequisite for the calibration of light detectors, whose detection efficiency strongly depends on the wavelength. During the SIQUEST project, we performed a relative calibration [24], carried out with the fibre exchange technique, that reached a relative standard uncertainty of 0.7 % for the ratio of detection efficiencies of two SPADs. Moreover, an absolute calibration [23] was demonstrated by a direct comparison of a SPAD with a low noise analogue detector via the substitution method. At high photon fluxes, the diminished nonlinearity of the apparent detection efficiency due to the sub-Poisson statistics proved the advantage of semiconductor quantum dots over laser light for applications in the field of quantum radiometry.

2.4.3. Characterization facilities for single-photon sources based on InGaAs quantum dots in the infrared spectral range

The sample characterisation facility being established and verified at NPL is schematically outlined in Figure 14. Some incidental optics such as mirrors to facilitate alignment and coupling lenses for the imaging spectrometer have been omitted to aid schematic clarity.

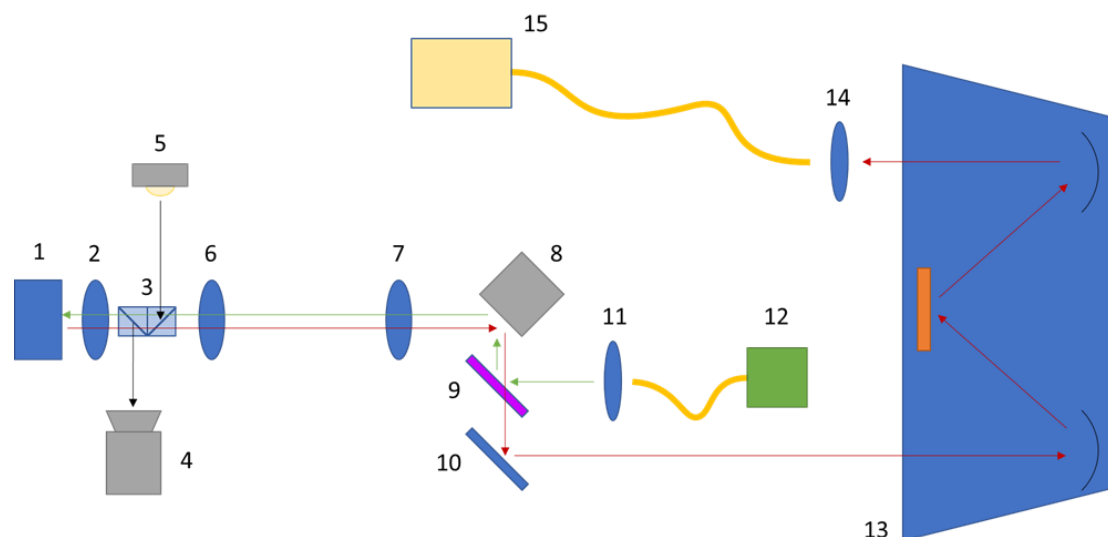


Figure 14. The experimental apparatus to perform measurements on QDs in the telecoms C band. 1. Continuous flow cryostat. 2. Aspheric (objective) lens. 3. Beam splitter pair for widefield imaging (removed during single photon data acquisition). 4. CMOS camera. 5. White LED. 6. Telecentric lens. 7. Telecentric lens. 8. Fast steering mirror. 9. Dichroic mirror. 10. Enhanced IR Au mirrors. 11. 850 nm collimation lens. 12. Fibre coupled 850 nm source. 13. Czerny-Turner spectrometer (iHR550). 14. Focussing lens for SMF28 fibre. 15. Multi-channel SNSPD system.

The system is designed to couple fluorescence from the quantum dot (QD) source to a set of superconducting nanowire single-photon detectors (SNSPDs). The sample is housed in a continuous flow cryostat (Janis ST-500), labelled (1) in Figure 14. Emission from cryostat is coupled into a 0.55 N.A. aspheric lens (Thorlabs AL1512-C), (2 in Figure 14). A pair of beam splitter cubes (3) can be inserted into the optical path for sample positioning. This allows white light (5) to be coupled in, and a wide field image to be projected onto the CMOS camera (4). Once the sample is correctly positioned these are removed, decoupling the camera and white light source from the system. A scanning mechanism comprised of two telecentric lenses (Thorlabs AC508-150-C-ML) are positioned in a 4-f arrangement (6,7). This allows the fast-steering mirror (Newport FSM), (8) to raster the angle of incidence of the optical path, scanning the focal region of the aspheric objective lens. A dichroic mirror (Thorlabs DMLP1180R), (9) couples the excitation source into the system. This is a CW 850 nm laser diode (Thorlabs LP852-SF30), (12), collimated by lens (11). Mirrors (10) couple the light into an imaging spectrometer (Horiba iHR550). Here the grating (600 lines/mm, 1000 nm blaze) can be used to spectrally select transmission lines or use the 0th order for imaging. The transmitted fluorescence is then coupled into an SMF28 fibre by a focussing lens (14), which is coupled to an SNSPD system (PhotonSpot).

The system is currently in the final stages of alignment and verification and should yield results in the near future.

2.4.4. Characterization facilities for single-photon sources based on molecules

Organic dye molecules are bright single photon sources which can be produced massively with nominally identical properties at low cost. They can be operated both at room and cryogenic temperature; in the latter case (below 4K) their quantum yield moves close to unity, and their

emission in the 00-zero phonon line becomes pronounced (branching ratio $\sim 0.3-0.5$ of the total emission) and Fourier-limited, i.e., they are able to provide highly indistinguishable photons.

To operate molecules as single photon sources, CNR has developed a simple procedure able to provide hundreds of useful emitters in a single sample. It consists in the dispersion of nanocrystals of anthracene doped with DBT [²⁵] over a gold mirror. With sufficiently low density of fluorophore, most of the nanocrystals contains zero or one emitter, and thanks to their average dimensions, this emitter can lay around 100nm far from the reflecting surface. This condition determines an effective redirection of the emission within a narrow cone around the polar axis, enhancing the collection efficiency even in case of limited numerical aperture [²⁶]. Such a configuration simplifies the search for good SPS, as the bright spot individuated performing a fluorescence map correspond with high probability to single emitters in the optimal conditions.

The SPS can be operated also at room temperature, with a similar performance except for spectral width (around 50nm) and no indistinguishability. However, optimal emission properties are obtained in case of cryogenic environment at 3K. We have verified in [²⁷] that emission properties are kept for operation up to 10K, except for indistinguishability.

The SPS does not require resonant pumping and cross-polarization setup in detection, high purity and indistinguishability is reported also under pulsed non-resonant excitation [²⁸].

The minimal setup to operate the SPS consists in a simple epi-fluorescence microscope:

- 1) a pulsed laser in the range 760-770nm, which is able to excite the molecules with 00-ZPL emission in the range 778nm-788nm (there is approximately 18nm between the two transitions) - Picoquant LDH-D-FA-765L,
- 2) a short pass filter (FSP in Figure 15a) to avoid residual emission from the laser in the wavelength range where the fluorescence signal is expected – Semrock FF01-769/41-25,
- 3) a half-wave plate to set the polarization of the pump light (molecules are well represented by linear dipoles orthogonal to the polar axis),
- 4) a high NA (~ 0.7) and high working distance (>5 mm) objective lens for epi-fluorescence detection – SigmaKoki PAL-50-NIR-HR-LC07,
- 5) a semi-reflective element with high transmission for the fluorescence (either a dichroic mirror or a highly unbalanced beam splitter) to separate collected light from excitation light,
- 6) a galvo-mirror or similar, integrated in a telecentric system of lenses, to scan the sample without the need of translational stage in the cryostat and/or for the objective lens – Thorlabs GVS002,
- 7) a high extinction long pass filter with transition at 790nm (able to work at lower wavelength by playing with incidence angle) and a steep Notch filter able to reflect in the 780-790nm spectral region – Semrock LP02-785RE and OptiGrate BNF-785-OD4-12.5M,
- 8) fibre launcher system to couple the fluorescence beam to a fibre. This is useful as spatial filter and to allow fibre-based circuitry for processing the collected photon flux - Elliot Scientific MDE120,
- 9) a fibre 50/50 beam splitter and a couple of single photon counting modules (SPAD) coupled to it, for the measurement of the collected photon flux intensity and purity – Thorlabs TN785R5A2 and Excelitas SPCM-NIR-14.

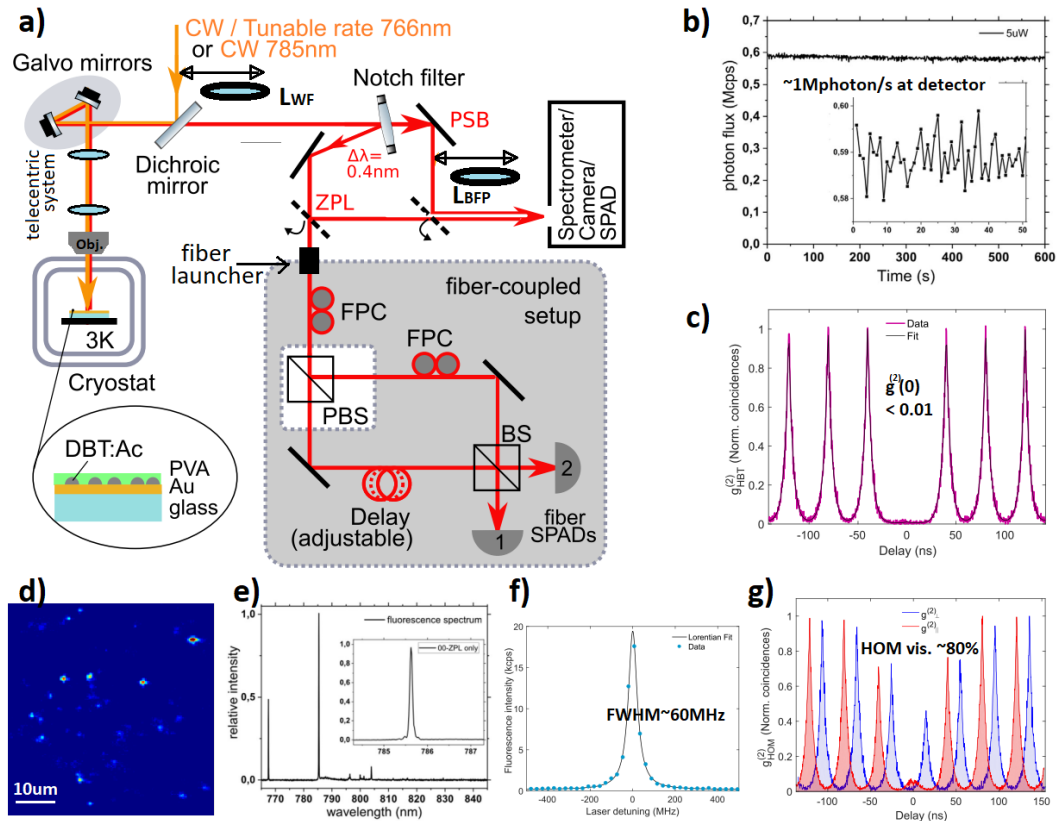


Figure 15. a) setup sketch [FPC: fibre polarization controller, (P)BS: (polarizing) beam splitter]; b) photon flux collected under continuous wave operation; c) purity evaluation under pulsed operation; d) fluorescence image of the SPS sample thanks to LWF ; e) emission spectrum of a single DBT molecule in anthracene nanocrystal at 3K, peak on the left is laser leakage; f) 00-ZPL resonance as probed via excitation spectroscopy; g) HOM interference (indistinguishability) under pulsed operation.

Additional useful elements which can be integrated in the setup are:

- 10) fibre-based elements to convert the simple fibre beam splitter into an unbalanced Mach-Zender interferometer with polarization manipulation tools for probing the indistinguishability of the collected photon flux- Thorlabs cage system, CCM1-PBS255, F260APC-780, FPC023,
- 11) a EMCCD camera/spectrometer system, for imaging and measuring the spectral distribution of the collected light – Andor Shamrock SR-303i-A,
- 12) a resonant laser (wavelength in the range of the pump laser + 18nm) with large mode-hop free frequency scan (like DFB or Littman-Metcalf ECDL), to probe the spectral width and the stability of the 00-ZPL line via excitation spectroscopy – Toptica LD-785-100-DFB,
- 13) a flippable lens in the excitation path (LWF in Figure 15a) to focus the laser light at the back entrance of the objective lens, for switching between confocal and wide-field illumination. This is a useful tool to perform a qualitative but fast exploration of the sample; Figure 15b is an example of such a fluorescence image,
- 14) a flippable lens in the detection path (LBFP in Figure 15a) to switch between object and back focal plane imaging,
- 15) an additional single photon counting module coupled to free space, to measure the photon flux before coupling it into the fibre.

2.5. Transportable single photon sources

2.5.1. Transportable single-photon source based on semiconductor quantum dots

Compact and user-friendly single-photon sources (SPSs) are key building blocks in photonic quantum technologies. In the best case they provide single photons on-demand at telecom wavelengths via single mode fibres. To reach this challenging goal we developed quantum dot (QD) based single-photon sources that can be used in a plug & play fashion with emission at around 930 nm and in the telecom O-band at 1.3 μm . The sources are on-chip fibre-coupled and are cooled by a compact Stirling cryocooler for stand-alone operation.

To build such SPSs self-assembled InGaAs QDs are grown by metal-organic chemical vapor deposition, usually with a back-side AlGaAs/GaAs distributed Bragg reflector (DBR) to enhance single-photon emission towards the collection optics and on-chip integrated fibres, respectively. Afterwards, in-situ electron beam lithography is used to select suitable QDs based on their emission intensity and emission wavelength and to integrate them deterministically with high process yield $> 90\%$ [29] into photonic nanostructures such as mesas [30], microlenses [31] and circular Bragg gratings [32] to maximize the photon extraction efficiency.

Next, the QD SPS must be on-chip fibre-coupled. This is a technically challenging processing step since it requires sub- μm alignment accuracy and high temperature stability for stable operation of the source at low temperature with maximum fibre-coupling efficiency. We have developed different schemes to tackle this issue by photoluminescence assisted alignment [33], interferometric alignment [34] and via the precise 3D printing of photonic elements and fibre-holders via two-photon lithography [35].

In the last fabrication step, the on-chip fibre-coupled SPS are integrated into a compact Stirling cryocooler with a base temperature of about 38 K within a 19"-rack housing, see Figure 16. For this purpose, they are mounted on the cooler's cold finger inside a vacuum chamber. The chamber has one or more fibre ports to excite the QD based SPS and to collect single-photon emission from the device. Excitation is usually provided by an integrated, and also fibre-coupled, pulsed diode laser via a fibre-based beam splitter. Emission of the QD-SPS is transmitted via the same beam splitter to the single-mode fibre output coupler of the stand-alone SPS. Fibre-based filters suppress the laser signal at the out but and a narrow bandpass filter transmits the target QD signal to the output coupler, where it is readily available for metrological measurements or for direct application in quantum cryptography [36].

The corresponding emission properties of a stand-alone single-mode fibre-coupled QD SPS emitting in the telecom O-band are presented Figure 17. Panel a) compares the emission detected at the fibre-output of the source with (orange trace) and without the integrated fibre-based bandpass filter (full-width at half maximum: 0.5 nm). With installed filter very clean emission at the target emission wavelength in the telecom O-band is observed. The count rate at the output of the single-mode fibre output depends on the excitation laser power and reaches close to 25 kHz at about 5 μW . Panel b) presents results on the single-photon emission properties of the source under pulsed quasi resonant p-shell excitation. The measured photon-autocorrelation functions show very pronounced photon anti-bunching associated with $g^{(2)}(0) = 0.10 \pm 0.01$. This reflects the excellent quantum nature of emission of the stand-alone SPS.

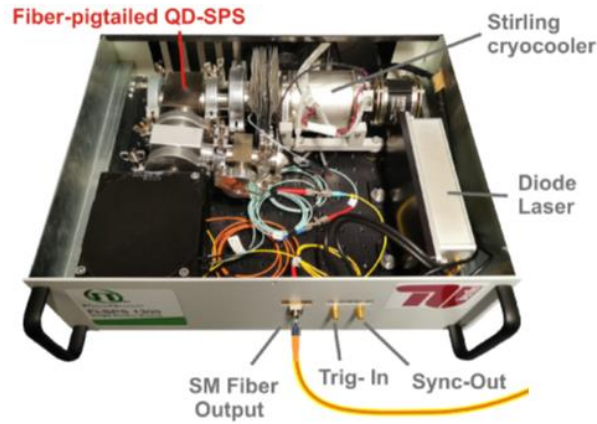


Figure 16. Image of a stand-alone fibre coupled SPS. The 19"-rack compatible on-chip fibre-coupled QD SPS is cooled to about 40 K by a compact Stirling cryocooler and can be pumped by an integrated diode laser. The device includes all necessary fibre-couplers and fibre-based filters to suppress emission from the exciting laser and to select emission of the telecom O-band quantum emitter available for direct usage in a quantum key distribution testbed via a standard single-mode fibre output coupler at the front panel of the SPS. Adopted from [36].

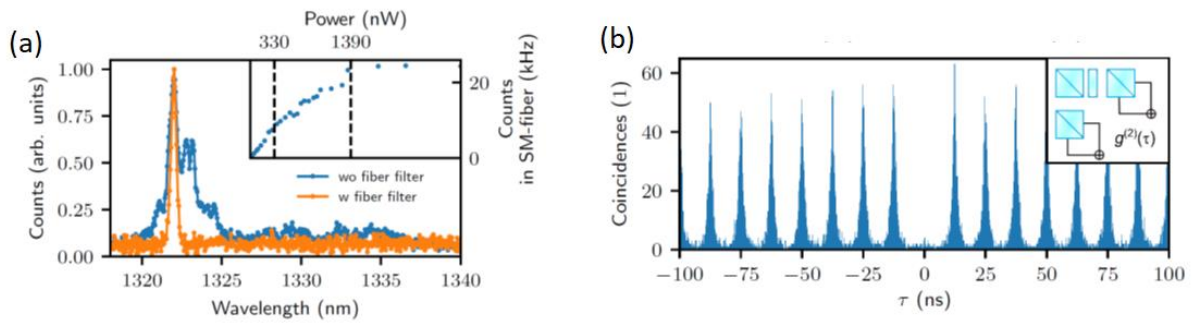


Figure 17. Emission properties of a transportable SPS emitting single-photons in the telecom O-band. a) Photoluminescence emission spectra at the single-mode fibre output of the quantum light source. b) Measured photon-autocorrelation function demonstrating clean single-photon emission with $g^{(2)}(0) = 0.10 \pm 0.01$. TUB1. Adopted from [36].

The achieved results clearly highlight the high potential of QD based structures to act as portable SPSs for applications in quantum metrology and quantum communication. Further optimization will focus on maximizing the single-photon flux by improving the fibre-coupling efficiency and to further improve the quantum nature of emissions also in terms of high photon indistinguishability.

2.5.2. Transportable single-photon source based on molecule and impurity centres in diamond

A compact single-photon source was developed and metrological characterized within the frame of the SIQUST project. It basically consists of a compact confocal setup that uses a NV-Centre or a single molecule as single-photon emitter. The setup is shown in Figure 18. Here a continuous wave (CW) laser with a wavelength of 532 nm is used for excitation of the single-

photon emitters. The laser beam is spectrally cleaned using a laser line filter and directed through a dichroic mirror to the microscope objective. The microscope objective focuses the excitation beam onto the sample using normal incidence or total internal reflection. The fluorescent light emitted by the emitter is then collected using the same microscope objective and passed through the dichroic mirror and long-pass filter to filter out the excitation laser. The beam is magnified using a 2:1 telescopic assembly, which also has an optional slot for a pinhole, and is then guided into an EMCCD camera or coupled via a lens to a multimode optical fibre. The single-photon purity of the emitters, second-order correlation function $g_2(t=0)$, is determined by an Hanbury Brown-Twiss (HBT) interferometer, which consists of a fibre beam splitter and two SPD modules. Thus, the single-photon emission is provided to the users via a MM fibre optic.

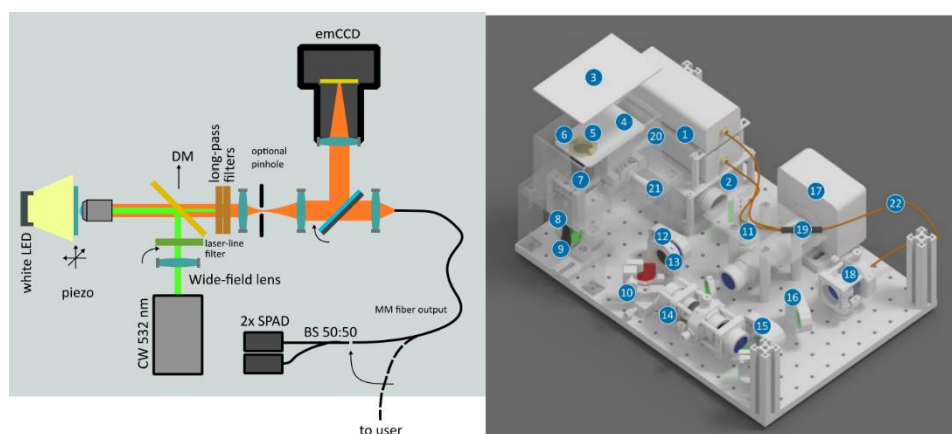


Figure 18. Left: Scheme of the compact single-photon setup. Right: Physical layout of the setup. Elements: 1) SPAD detectors, 2) excitation laser, 3) cover lid with LED illumination, 4) sample holder plate, 5) sample - cover glass with emitters, 6) small magnets, 7) microscope objective, 8) coarse Z-positioner of the objective, 9) 45-deg mirror, 10) dichroic mirror, 11) steering mirror, 12) optional wide-field lens, 13) laser-line filter, 14) magnifying telescope with optional pinhole, 15) long-pass filters, 16) flip-mirror, 17) emCCD camera, 18) fibre-coupler, 19) multimode 50:50 fibre beam-splitter, 20, 21) coarse sample X,Y-positioner, 22) output multimode fibre.

Figure 19 shows the fluorescence emission and second order correlation function $g_2(t_0)$ obtained for a single molecule (terrylene in p-terphenyl crystal). The excitation of the terrylene molecule is carried out by using total internal reflection. The $g_2(t=0)$ value is around 0.2, which demonstrates the antibunching characteristic of the emitted photons. The maximum photon flux rate achieved with this setup using a single molecule is about 1 Mphoton/s.

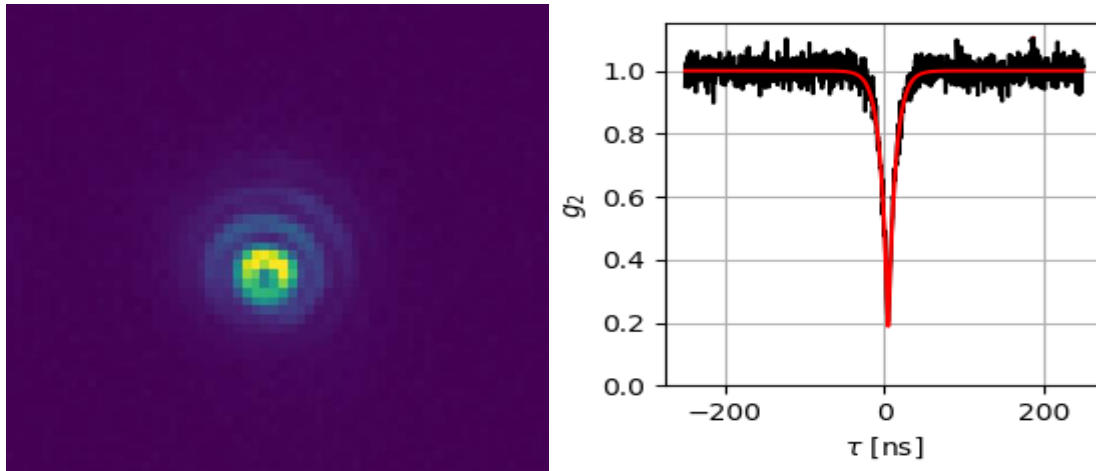


Figure 19. Left: Image of the fluorescence pattern of a single molecule (terrylene in p-terphenyl crystal). Right: Second order correlation function $g_2(t=0)$.

2.6. Joint activities

2.6.1. Calibration of ISTED

One of the objectives of this project was to facilitate the use of portable SPSs and reference detectors. The PQED cryostat (See section 2.2) is suitable as travelling reference detector despite of its relatively large size. Therefore, in order to calibrate other candidate reference and SPAD detectors using the available SPS at PTB, the PQED was shipped to Germany. We conducted measurements with attenuated laser and single photon source [see section 2.4.2]. The comparison measurements of a reference detector from CMI against PQED with attenuated laser was successful down to 20 pW that corresponds to about 100 million of photons per second at 933 nm (

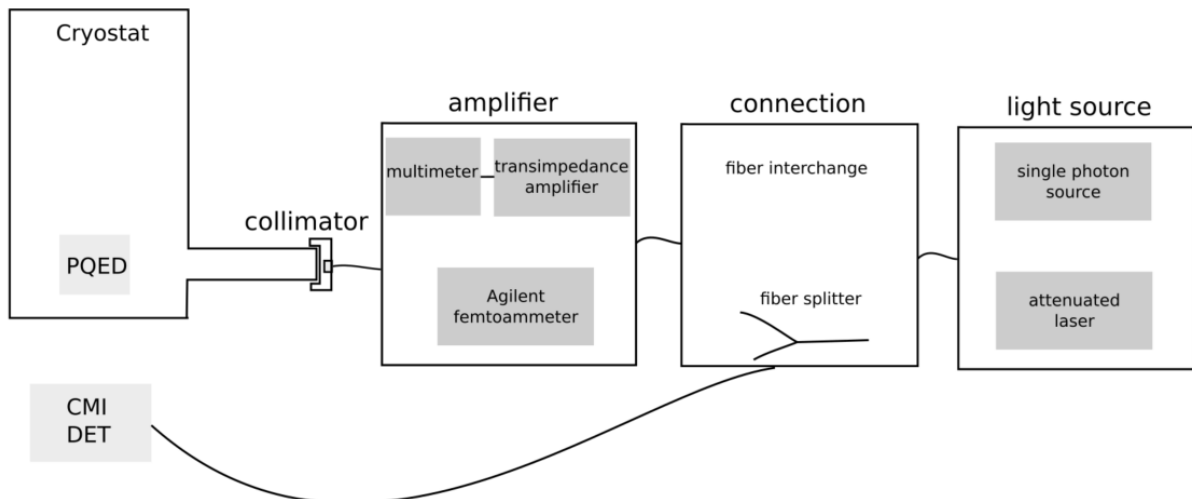


Figure 20). However, it was revealed that the elevated dark signals and noise level of PQED signal prevented reliable comparison measurements with SPAD detector at lower photon rates.

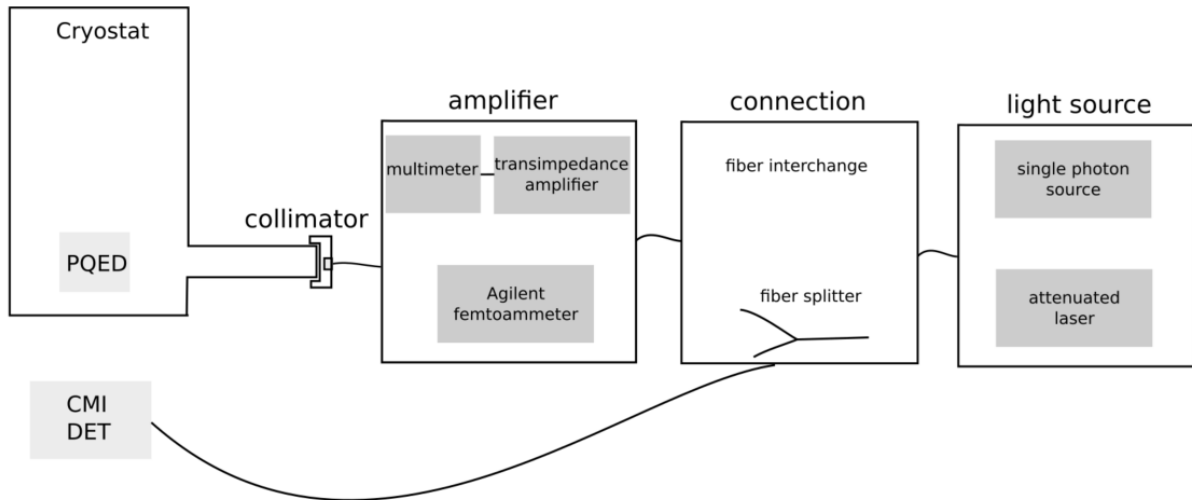


Figure 20. Schematic drawing of setup for low flux measurement with PQED and CMI detector at PTB

2.6.2. Detection efficiency comparison

In this section, we report on pilot studies for the measurements of detection efficiency of SPADs in the 1550 nm region, exploited a free-running InGaAs/InP SPAD-based detector.

Single-photon avalanche diodes (SPAD) based on InGaAs/InP semiconductor materials are the most exploited detectors in many quantum technologies [37, 38]. The successful development of such new technologies and products requires the solution to a number of metrological challenges; for this reason, a metrological characterization in terms of detection efficiency, dead time, after pulsing and dark counts of single photon detectors is mandatory. A pilot study to compare different detection efficiency measurement strategies at the wavelength of 1550 nm was performed by four European National Metrology Institutes: CMI, INRIM, NPL and PTB [39]. The device under test was a commercial free-running fibre-coupled InGaAs/InP single-photon detector. The setup and the reference standard used as well as a detailed estimation of the measurement uncertainty of the detection efficiency was compared. The DUT was a fibre pigtailed free running SPAD (Id Quantique ID220), with nominal detection efficiency of 10% and dead time D of 10 μ s. All the participants provided quantum efficiency measurement with the detector illuminated by a pulsed laser source, a commercial short-pulse laser source (ID Quantique, id300), which is based on a Distributed-feedback laser diode at 1550 nm. The measurement was carried out with the common repetition rate of 110 KHz. The exact wavelength of the source is measured with an optical spectrum analyser (Anritsu MS974 OA). The measurement principle used by all participating laboratories for determining the detection efficiency of the InGaAs/InP SPAD detector was based on the substitution method. In a general scheme, adopted by all the participants, the output of the laser was sent to a device that provide a variable calibrated attenuation to attenuate light at single photon level. The detection efficiency was estimated by comparing the optical power measured by the DUT with the incident mean optical power per laser pulse measured with an analogue calibrated detector.

A new model to evaluate efficiency in presence of dead time and dark count effects of pulsed light illuminating a free-running detector was introduced [39] and then extended to an extremely wide variety of experimental conditions [40]. The detection efficiency was measured by each NMI, in a range of mean photon number per pulse between 0.01 and 2.4,

and standard uncertainty was reported. Results show consistency between the different measurement strategies.

2.6.3. $g^{(2)}$ -comparison using Hanbury Brown Twiss interferometer

In this section, we report on pilot studies for the measurements of source photon statistics for SPSs at telecom wavelength, together with an analogue comparison characterisation in the VIS-NIR regime, and the realisation of pilot measurement comparisons to validate the techniques developed.

As a route to the validation of the measurement facilities and infrastructure, four European NMIs (INRIM, PTB, NPL and CMI) performed two joint measurements at INRIM labs of the Glauber second-order auto-correlation function ($g^{(2)}$) of pseudo single-photon sources in two different configurations: CW heralded SPS at telecom wavelength [41] and NV-based SPS in pulsed excitation in the visible/near infrared [42]. Measurement protocols and procedures were developed on purpose.

For both joint measurement, the source output is addressed to a 50:50 fibre beam splitter (FBS) whose outputs are sent to two Hanbury Brown & Twiss (HBT) interferometers, one belonging to INRiM and the other to the guest NMI (PTB or NPL), allowing simultaneous data collection between INRiM and the guest NMI to avoid mismatch due to some drift in the HSPS output over time.

The pilot study towards a comparison on the measurements of $g^{(2)}$ in the telecom range [41] achieved a good agreement within the uncertainty. The source used for this test was a CW heralded single-photon source (HSPS) emitting real single photons at 1550 nm.

In this case (for a scheme of the setup, refer to [41]), the source uses a CW laser (532 nm) pumping a 10 mm \times 1 mm \times 10 mm periodically-poled lithium niobate (PPLN) crystal to produce non-degenerate SPDC. Signal and idler photons, respectively with wavelengths 1550 nm and 810 nm, are filtered and coupled to single-mode fibres (SMF). The detection of an idler photon by the SPCM-AQR silicon single-photon avalanche detector heralds the arrival of a 1550 nm signal photon, addressed to a 20 m long single-mode optical fibre connected to an electro-optical shutter (OS) operated by a fast pulse generator, which is in turn controlled by a field programmable gate array (FPGA). For each heralding signal, the FPGA operates the pulse generator in order to open the HSPS output channel, i.e., OS channel A, for a time window of 7 ns in correspondence of the passage of a 1550 nm photon.

In this experiment, every HBT is composed of two infrared InGaAs-InP SPADs, be they free-running or gated (when gated, the SPADs are triggered by the same FPGA signal opening the OS), whose outputs are sent to time-tagging coincidence electronics. Actually, the parameter we evaluate to characterize the emission of our source is $\alpha = P_{12}/(P_1 \cdot P_2) \cong g^{(2)}(0)$, where P_{12} and P_i ($i=1,2$) are, respectively, the probability of a coincidence count between the two HBT SPADs and the photon count probability for each of the HBT SPADs (dark counts subtracted). After a careful analysis of the setup parameters for a proper evaluation of the uncertainties associated to our measurements, we obtained the results below.

	α (INRIM)	α (NPL)	α (PTB)
INRIM-PTB	0.016 ± 0.006	-	0.04 ± 0.05
INRIM-NPL	0.013 ± 0.008	0.02 ± 0.02	-

As visible in the table above, the results of the whole measurement campaign (involving different measurement setups and data collection methodologies) are all in agreement within the experimental uncertainties reported (coverage factor: $k = 1$).

Concerning the pilot study towards a comparison on the measurements of $g^{(2)}(0)$ in the VIS-NIR regime [42], the source used was a pulsed single photon source based on nitrogen-vacancy centres in diamond.

The experimental setup (for a scheme of the setup, refer to [42]) is composed of a laser-scanning confocal microscope whose signal, i.e. the fluorescence emitted by a single NV centre of negative charge (with emission in a broad spectral band starting approximately at 630 nm and ending at 750 nm), is sent to the HBTs of the partners participating in the joint measurement. The excitation light, produced by a pulsed laser (48 ps FWHM, 560 pJ per pulse) emitting at 532 nm with a repetition rate $R = 2.5$ MHz was focused by a 100X oil-immersion objective on a nano-diamond (ND) sample. The optical filters used were a notch filter at 532 nm and two long-pass filters (FEL600 and FEL650). The photoluminescence signal (PL), thus occurring in a 650–750 nm spectral range, was collected by a multimode fibre and split by a 50:50 beam-splitter (BS). As stated above, each end of the BS was connected to a separate HBT setup used for the joint measurement. In particular each facility was composed of:

- INRiM: a fused 50:50 fibre beam-splitter connected to two Excelitas SPCM-AQR-14-FC single-photon avalanche detectors (SPADs). Single and coincidence counts were sampled via ID Quantique ID800 time-to-digital converter (60 ps time resolution).
- NPL: a fused 50:50 fibre beam-splitter connected to two Perkin-Elmer SPCM-AQR-14-FC single-photon avalanche detectors (SPADs). Coincidence counts were sampled via PicoQuant HydraHarp 400 multichannel picosecond event timer (1 ps time resolution).
- PTB: a fused 50:50 fibre beam-splitter connected to two Excelitas SPCM-AQR-14-FC single-photon avalanche detectors (SPADs). Single and coincidence counts were sampled via PicoQuant HydraHarp 300 multichannel picosecond event timer (4 ps time resolution).

The validity of the technique is demonstrated by compatibility of the results obtained by the three partners (see table below), demonstrating a system-independent (and unaffected by the non-ideality of the apparatus), estimate of $g^{(2)}(0)$, emission lifetime ($\tau = 15.34 \pm 0.08$ ns and their uncertainty).

	α (INRIM)	α (NPL)	α (PTB)
INRIM-PTB	0.079 ± 0.009	-	0.076 ± 0.007
INRIM-NPL	0.065 ± 0.005	0.068 ± 0.005	-

3. Summary and outlook

In this paper we have reported on the development of the measurement capabilities in the European national metrology institutes with respect to the metrological characterization and measurement traceability for single-photon sources. These developments were carried out within the frame of the joint research project Single-photon sources as new quantum standards (SIQUST, 17FUN06), which also triggered further developments in the metrology partner institutes. The setups and devices included detectors, detector characterization setups, transportable single-photon sources, setups for the characterization of the total spectral radiant

flux and the photon statistics of single-photon sources as well as laser sources for the operation of single-photon sources.

Next steps into the direction of exploiting quantum metrology in national metrology institutes will be the implementation of measurement infrastructure for application of single-photon sources and also of entangled photon sources in quantum metrology, e.g., quantum imaging and quantum-based microscopy. Part of this work will be carried out in the follow-up joint research project SEQUME (Single and entangled photon sources for quantum metrology [⁴³]).

4. References

¹ <https://www.siqust.eu/>

² Mountford, J., Porrovecchio, G., Smid, M., Smid, R.: Development of a switched integrator amplifier for high-accuracy optical measurements. *Appl. Opt.* 47(31), 5821 (2008)

³ Porrovecchio, G., Smid, M., Lopez, M., Rodiek, B., Kück, S., Hofer, H., Comparison at the sub-100 fW optical power level of calibrating a single-photon detector using a high-sensitive, low-noise silicon photodiode and the double attenuator technique. *Metrologia* (53), 1115-1122 (2016).

⁴ Sildoja, M., Manoocheri, F., Merimaa, M., Ikonen, E., Müller, I., Werner, L., Gran, J., Kübarsepp, T., Smid, M., Rastello, M.L.: Predictable quantum efficient detector: I. Photodiodes and predicted responsivity. *Metrologia* 50(4), 385 (2013)

⁵ Müller, I., Johannsen, U., Linke, U., Socaciu-Siebert, L., Smid, M., Porrovecchio, G., Sildoja, M., Manoocheri, F., Ikonen, E., Gran, J., et al.: Predictable quantum efficient detector: II. Characterization and confirmed responsivity. *Metrologia* 50(4), 395 (2013)

⁶ Dönsberg, T., Sildoja, M., Manoocheri, F., Merimaa, M., Petroff, L., Ikonen, E.: New source and detector technology for the realization of photometric units. *Metrologia* 51(3), 197 (2014)

⁷ Hansen, T.: Silicon UV-photodiodes using natural inversion layers. *Phys. Scr.* 18(6), 471 (1978)

⁸ Salfner, K., Dönsberg, T., Porrovecchio, G., Smid, M., Nield, K., Nevas, S.: Characterization of a room temperature predictable quantum efficient detector for applications in radiometry and photometry. *Metrologia* 55(5), 654 (2018)

⁹ Dönsberg, T., Pulli, T., Poikonen, T., Baumgartner, H., Vaskuri, A., Sildoja, M., Manoocheri, F., Kärhä, P., Ikonen, E.: New source and detector technology for the realization of photometric units. *Metrologia* 51(6), S276 (2014)

¹⁰ Pulli, T., Dönsberg, T., Poikonen, T., Manoocheri, F., Kärhä, P., Ikonen, E.: Advantages of white LED lamps and new detector technology in photometry. *Light Sci. Appl.* 4(9), 332 (2015)

¹¹ Dönsberg, T., Mäntynen, H., Ikonen, E.: Optical aperture area determination for accurate illuminance and luminous efficacy measurements of LED lamps. *Opt. Rev.* 23(3), 510 (2016)

¹² Dönsberg, T., Manoocheri, F., Sildoja, M., Juntunen, M., Savin, H., Tuovinen, E., Ronkainen, H., Prunnila, M., Merimaa, M., Tang, C.K., et al.: Predictable quantum efficient detector based on n-type silicon photodiodes. *Metrologia* 54(6), 821 (2017)

¹³ Gran, J., Kübarsepp, T., Sildoja, M., Manoocheri, F., Ikonen, E., Müller, I.: Simulations of a predictable quantum efficient detector with PC1D. *Metrologia* 49(2), S130 (2012)

¹⁴ Manoocheri, F., Sildoja, M., Dönsberg, T., Merimaa, M., Ikonen, E.: Low-loss photon-to-electron conversion. *Opt. Rev.* 21(3), 320 (2014)

¹⁵ Geist, J., Brida, G., Rastello, M.L.: Prospects for improving the accuracy of silicon photodiode self-calibration with custom cryogenic photodiodes. *Metrologia* 40(1), S132 (2003)

-
- ¹⁶ Vaigu, A., Porrovecchio, G., Chu, X.L., Lindner, S., Smid, M., Manninen, A., Becher, C., Sandoghdar, V., Götzinger, S., Ikonen, E.: Experimental demonstration of a predictable single photon source with variable photon flux. *Metrologia* 54(2), 218 (2017)
- ¹⁷ Manoocheri, F., Dönsberg, T., Sildoja, M., Smíd, M., Porrovecchio, G., Ikonen, E.: Liquid nitrogen cryostat for predictable quantum efficient detectors. *J. Phys. Conf. Ser.* 972(1), 012021 (2018)
- ¹⁸ Porrasmäa, S., Dönsberg, T., Manoocheri, F., Ikonen, E., “Predictable quantum efficient detector for low optical flux measurements”, *Optical Review* (2020) 27:190–194 <https://doi.org/10.1007/s10043-020-00580-1>
- ¹⁹ Sildoja, M., Manoocheri, F., Ikonen, E.: Reflectance calculations for a predictable quantum efficient detector. *Metrologia* 46(4), S151 (2009)
- ²⁰ T Kübarssepp et al (1996), Characterization of a polarization-independent transmission trap detector, *Appl Opt*, 36, pp 2807-2812
- ²¹ A Pokatilov et al, Low-noise miniature photodetector as a transfer standard for SPAD calibration in the visible wavelength range, *Proc. of NEWRAD 2017* (Tokyo, Japan, 2017)
- ²² J. Christinck et al., *Appl. Phys. B.* 126, 161 (2020)
- ²³ H. Georgieva et al. *Opt. Express* 29 15 (2021)
- ²⁴ H. Georgieva et al. *Metrologia* 57 5 (2020)
- ²⁵ S. Pazzagli et al., *ACS Nano* 12 (5), 2018
- ²⁶ S. Checcucci et al., *Light:S&A* 6, 2017
- ²⁷ P. Lombardi et al., *Adv. Quantum Technol.* 3 (2), 2020
- ²⁸ P. Lombardi et al., *Appl. Phys. Lett.* 118 (20), 2021
- ²⁹ M. Gschrey et al., In situ electron-beam lithography of deterministic single-quantum-dot mesa-structures using low-temperature cathodoluminescence spectroscopy, *Applied Physics Letters* 102, 251113 (2013)
- ³⁰ N. Srocka et al., Deterministically fabricated strain-tunable quantum dot single-photon sources emitting in the telecom O-band, *Applied Physics Letters* 117, 224001 (2020)
- ³¹ M. Gschrey et al., Highly indistinguishable photons from deterministic quantum-dot microlenses utilizing three-dimensional in situ electron-beam lithography, *Nature Communications* 6, 1 (2015)
- ³² J. Schall et al., Bright Electrically Controllable Quantum-Dot-Molecule Devices Fabricated by In Situ Electron-Beam Lithography, *Advanced Quantum Technologies* 4, 2100002 (2021)
- ³³ A. Schlehahn et al., A stand-alone fiber-coupled single-photon source, *Scientific Reports* 8, 1 (2018)
- ³⁴ K Żółnacz et al., Method for direct coupling of a semiconductor quantum dot to an optical fiber for single-photon source applications, *Optics express* 27, 26772 (2019)
- ³⁵ L. Bremer et al., Quantum dot single-photon emission coupled into single-mode fibers with 3D printed micro-objectives, *APL Photonics* 5, 106101 (2020)
- ³⁶ T. Gao et al., A Quantum Key Distribution Testbed using a Plug&Play Telecom-wavelength Single-Photon Source, arXiv:2105.03473; accepted for publication in *Applied Physics Reviews* (2022)
- ³⁷ Hadfield RH (2009) *Nat Photonics* 3:696–705
- ³⁸ Stucki D et al (2001) *J Mod Opt* 48(13):1967–1981
- ³⁹ Lopez M et al (2020) *EPJ Quantum Technol.* 7: 14
- ⁴⁰ Georgieva H et al (2021) *Appl. Phys. Lett.* 118, 174002
- ⁴¹ Rebufello E et al (2019) Towards a standard procedure for the measurement of the multi-photon component in a CW telecom heralded single-photon source. *Metrologia* 56:025004
- ⁴² E. Moreva et al. *Metrologia* 56, 015016 (2019)
- ⁴³ <https://www.sequme.eu/>